Tuning the ATP-ATP and ATP-disordered protein interactions in high ATP concentration by altering water models

Mori, Toshifumi
Institute for Materials Chemistry and Engineering, Kyushu University

Yoshida, Norio
Graduate School of Informatics, Nagoya University

https://hdl.handle.net/2324/7159646

Tuning the ATP–ATP and ATP–disordered protein interactions in high ATP concentration by altering water models

Toshifumi Mori[1, 2, a)] and Norio Yoshida[3]

[1)] *Institute for Materials Chemistry and Engineering, Kyushu University, Kasuga, Fukuoka 816-8580, Japan*

[2)] *Department of Interdisciplinary Engineering Sciences, Interdisciplinary Graduate School of Engineering Sciences, Kyushu University, Kasuga, Fukuoka 816-8580, Japan*

[3)] *Graduate School of Informatics, Nagoya University, Chikusa, Nagoya, 464-8601, Japan*

The ATP–protein interactions have been of great interest since the recent experimental finding of ATP's role as a hydrotrope. The interaction between ATP and disordered proteins is fundamental to the dissolution of protein aggregates and regulation of liquid-liquid phase separation by ATP. Molecular dynamics simulation is a powerful tool in analyzing these interactions in molecular detail but often suffer from inaccuracies in describing disordered proteins and ATPs in high concentrations. Recently, several water models have been proposed to improve the description of the protein disordered states, yet how these models work with ATP have not been explored. To this end, here we study how water models affect ATP and alter the ATP–ATP and ATP–protein interactions for the intrinsically disordered protein, α-Synuclein. Three water models, TIP4P-D, OPC, and TIP3P, are compared, while the protein force field is fixed to ff99SBildn. The results show that ATP over-aggregates into a single cluster in TIP3P water, but monomers and smaller clusters are found in TIP4P-D and OPC waters. ATP–protein interaction is also over-stabilized in TIP3P, whereas repeated binding/unbinding of ATP to α-Synuclein is observed in OPC and TIP4P-D waters, which is in line with the recent NMR experiment. The adenine ring-mediated interaction is found to play a major role in ATP–ATP and ATP–protein contacts. Interestingly, changing Mg^{2+} into Na^+ strengthened the electrostatic interaction and promoted ATP oligomerization and ATP–α-Synuclein binding. Overall, the current study shows that changing the water model can be an effective approach to improve the properties of ATP in high concentration.

a)Electronic mail: toshi_mori@cm.kyushu-u.ac.jp

I.   INTRODUCTION

Adenosine triphosphate (ATP) serves as an energy currency in living cells. ATP consists of an adenine base, ribose sugar, and triphosphate groups, and often exists as a complex with metal cations such as Mg^{2+}. While ATP at $\sim$100 μM is sufficient for most ATP-utilizing enzymes, the physiological concentration of ATP (1–10 mM) is much higher by 10 to 100 fold[1–4], implying that ATP may have other physiological functions as well. Recently, Patel *et al.* have shown that high concentration of ATP ($\sim$10 mM) can dissolve protein aggregates and inhibit protein aggregation.[5] A number of experiments have further shown that ATP interacts with a variety of proteins in a nonspecific manner[6–12]. Thus, ATP can stabilize protein native state, improve protein solubility, and regulate liquid-liquid phase separation (LLPS) by acting as an effective cosolvent, and act as a hydrotrope[13,14]. Interestingly, the proteins studied in these works are not ATP-utilizing proteins, i.e., do not have any ATP binding site. Nevertheless, both adenine base and triphosphate groups of ATP were indicated to contribute to the ATP–protein interactions but the molecular basis remains unclear. Furthermore, while Mg^{2+} ion is often accompanied with ATP to balance the negatively charged triphosphate moiety, it was found that ATP can bind to proteins even without Mg^{2+}[15,16].

Molecular dynamics (MD) simulations have been performed to reveal the ATP–protein as well as ATP–ATP interactions in molecular detail.[16–24] For instance, the studies of ATP binding to proteins in the native state[16,17] have indicated that ATP molecules bind to the loop regions where the conformation is flexible. Arginine (Arg) was indicated to bind ATP molecules most frequently[17], possibly due to the positive charge of Arg which attracts ATP's strongly negative charge. Furthermore, ATP molecules themselves were found to aggregate strongly, form clusters around the protein, and thereby bind to proteins both directly and indirectly. MD simulations to understand the dissolution of protein aggregates have also been performed[23,24], which indicated that the adenine moiety of ATP is important to interact with the disordered protein aggregates. The mechanism of ATP to inhibit the fibrillation of intrinsically disordered proteins have also been studied using short peptides and model molecules[19–22], which also suggested that adenine part of ATP is interacting with the proteins more frequently than the hydrophilic triphosphate moiety.

On the other hand, the studies of ATP–ATP interactions using MD simulations have indi-

cated that ATP molecules tend to over-aggregate compared to the experimentally measured binding constant[18–20]. To circumvent this discrepancy, charge scaling of the atoms in ATP by a factor of 0.6-0.7 has been suggested.[19,20] While this scaling improves the ATP–ATP interaction and brings the binding constant similar to that in experiment, this also deteriorates the ATP–protein potential and changes the molecular mechanism of ATP binding to proteins.

Understanding how ATP molecules interact with the proteins in the disordered state is essential to reveal the mechanism of aggregate dissolution and LLPS. Yet, it has been realized that conventional protein force fields are not sufficient in describing the protein unfolded states.[25–29] In particular, the simulated radius of gyration of the unfolded protein is often too small compared to the experimentally measured value[25,26]. This issue has partially been attributed to the widely used water model, TIP3P, which is known to be inaccurate in describing the solubilized molecules as well as reproducing water properties. Recently, Piana *et al.*[30] and Shabane *et al.*[31] have developed the TIP4P-D and OPC water models, respectively, to improve the properties of the unfolded proteins. These results imply that the over-aggregation of ATP molecules may also be improved by altering the water model rather than modifying the ATP force field.

To this end, here we study how water models affect the ATP aggregation propensity and ATP–protein interactions for the protein in the disordered state. We study α-Synuclein (α-Syn), which is a typical intrinsically disordered protein. The interaction between α-Syn and ATP has been studied experimentally in molecular detail[15]. The effect of Mg^{2+} ion to the ATP aggregation and ATP binding to protein has also been discussed. Here we focus on revealing how water model alters the properties of ATP, rather than performing a comprehensive study of different combinations of protein, water, and ATP force fields. Thus, we compare three water models, i.e., TIP4P-D, OPC, and TIP3P, while the protein and ATP force fields are fixed to keep the ATP–protein potential unchanged. By performing multiple $\sim \mu s$ MD simulations for each system to account, we discuss how the ATP cluster sizes change dynamically over time, what contributes to stabilizing the ATP–ATP and ATP–protein interactions, and how these properties depend on the water models.

II.   COMPUTATIONAL DETAILS

To study the ATP–ATP interactions in different water models, 18 ATP molecules were randomly placed in a box of $126 \times 126 \times 126$ Å^3 using PACKMOL[32]. This sets the concentration of ATP molecule to ~ 15 mM. The box was subsequently filled with water molecules. 18 Mg^{2+} were then added, and after neutralizing the system with Na^+ ions, 180 Na^+ and Cl^- ions were added to set the ion concentration to 150 mM. To examine the effect of magnesium ions, the systems without Mg^{2+} ions were also prepared. A separate setup adding 36 additional Na^+ ions instead of 18 Mg^{2+} ions was also prepared.

Since sampling the structure of intrinsically disordered protein throughly requires extensive MD simulations on the order of >10 μs even without ATP molecules[30], here we rather focus our study on the ATP distribution about a few representative structures of α-Syn. The structures of α-Syn were extracted from the ~ 11 μs trajectory by Piana et al.[30] which used Anton. Since His50 was protonated in their simulations, we followed the same protonation state. We used the trajectory generated from Amber 12 and TIP4P-D force fields which showed large radius of gyration. We extracted three representative unfolded structures from the trajectory (Fig. S1) and used them as the initial structures. Each α-Syn structure, together with 18 ATP molecules, was randomly placed in a box of $126 \times 126 \times 126$ Å^3 using PACKMOL[32], and either 18 Mg^{2+} or 36 Na^+ ions were added. Note that this box size is much larger than that used for α-Syn by Piana et al.[30] (where they used a $\sim 100 \times 100 \times 100$ Å^3 box), but was adopted here to keep the number of ATP molecules the same as above. Each system was then neutralized using Na^+ ions, and subsequently filled with water. Na^+ and Cl^- ions were further added to set the NaCl concentration to 150 mM. Amber ff99SBildn force field was used for the protein[33], and ATP was treated with the force field by Meagher et al.[34]. Systems with three different water models, i.e., TIP4P-D[30], OPC[31], and TIP3P, were prepared separately, and the monovalent and divalent ions were described by the force fields developed by Joung and Cheatham[35] and Li and Merz[36], respectively, which have been tuned for each water model in Amber 20[37]. Long-range electrostatic interactions were calculated using the particle mesh Ewald method, and short-range non-bonded interactions were cut off at 10.0 Å.

Each system was initially energy minimized for 3000 steps while restraining the heavy atoms, and heated up to 300 K in 100 ps. Subsequently, constant-NPT (300 K, 1 atm)

simulation was run for 500 ps while restraining the heavy atoms of α-Syn and ATP molecules with a weak force constant of 1 kcal mol^{-1} Å^{-2}. The restraint on the heavy atoms were then removed, and another 10 ns constant-NPT simulation was conducted to finalize equilibration. The production simulations were then performed under the constant-NPT (300 K, 1 atm) condition for 1.2 μs. The temperature was maintained using a Langevin thermostat with a collision frequency of 1.0 ps^{-1}, and the pressure was controlled using the Berendsen barostat. Note that while the volume of the system changes when the constant-NPT condition is turned on, the final concentrations of ATP and Mg^{2+} changed only by $\sim$3 %. The simulations were performed using the GPU version of PMEMD module in the Amber 20 program package.[37,38]

III.   RESULTS AND DISCUSSION

ATP–ATP interactions and ATP clustering propensity

First we compare how different water models affect the dynamics and oligomerization trend of ATP molecules. ATP molecules are counted to be in contact when the shortest inter-atomic distance between two ATP molecules are within 4 Å; the ATP molecules in contact are then assigned to the same cluster. Fig. 1 shows how the sizes of ATP clusters change during the representative trajectories. The results for the other trajectories with and without Mg^{2+} ions are given in Figs. S2 and S3, respectively. The figures show that, in the presence of Mg^{2+}, the cluster sizes increase almost monotonically in TIP3P water and eventually converge to a single cluster within 500 ns. In contrast, the clusters in TIP4P-D and OPC waters change dynamically, and the sizes are diverse. Similar trend is seen when Mg^{2+} ions are absent, though the ATP clusters tend to be formed more rapidly and stably.

To compare the cluster sizes in more detail, the ATP cluster size distributions are summarized in Fig. 2. Since the cluster sizes changed drastically in the beginning of each trajectory, hereafter the trajectory segment from 0.2 μs to 1.2 μs are used when taking the time averages. This result shows that ATPs in TIP3P water mostly form a single 18-mer. In TIP4P-D and OPC waters, monomers appear to be the major species when Mg^{2+} is present, but dimers and small oligomers become more favorable when Mg^{2+} is absent. The ATPs in TIP4P-D water tend to oligomerize more frequently than those in OPC water. Here we note that the monomeric form is experimentally expected to be dominant in the current
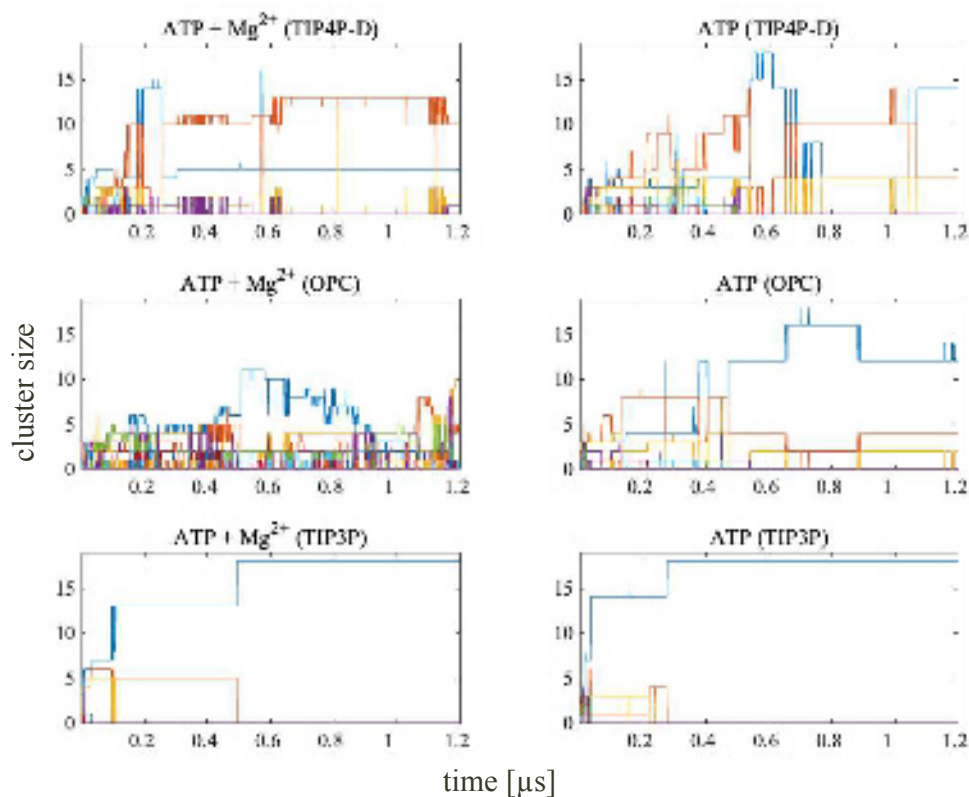
FIG. 1. Time evolution of the ATP cluster sizes in the presence (left) and absence (right) of Mg^{2+} ions in different water models from the representative trajectories. Top, center, and bottom rows denote the results for TIP4P-D, OPC, and TIP3P waters, respectively. The clusters are colored based on the smallest residue ID of the ATP in each cluster to follow the dynamic changes of the cluster component. The change in color indicates that the components of the cluster changed, i.e., either the ATP with the smallest residue ID left or another ATP with smaller residue ID entered the cluster.

ATP concentration[14,15]; for instance, in the experimental condition of 10 mM ATP, 10 mM magnesium chloride, and 150 mM sodium chloride, similar to the current simulations, 84% of ATP–Mg complex is estimated to exist in the monomeric form.[15,39–41] Fig. 2 shows that 7, 12, and 0 % of the ATPs exist as monomers in TIP4P-D, OPC, and TIP3P waters, respectively. TIP3P water thus drastically overestimates the oligomerization trend. The TIP4P-D and OPC waters, on the other hand, are still biased towards oligomers, but the deviation from experiment is greatly improved compared to the TIP3P case.

To analyze the molecular origin of ATP–ATP interactions in more detail, the joint distribution as a function of adenine–adenine and triphosphate–triphosphate distances between ATP molecules are plotted in Fig. 3. Here, the distance is defined as the shortest inter-
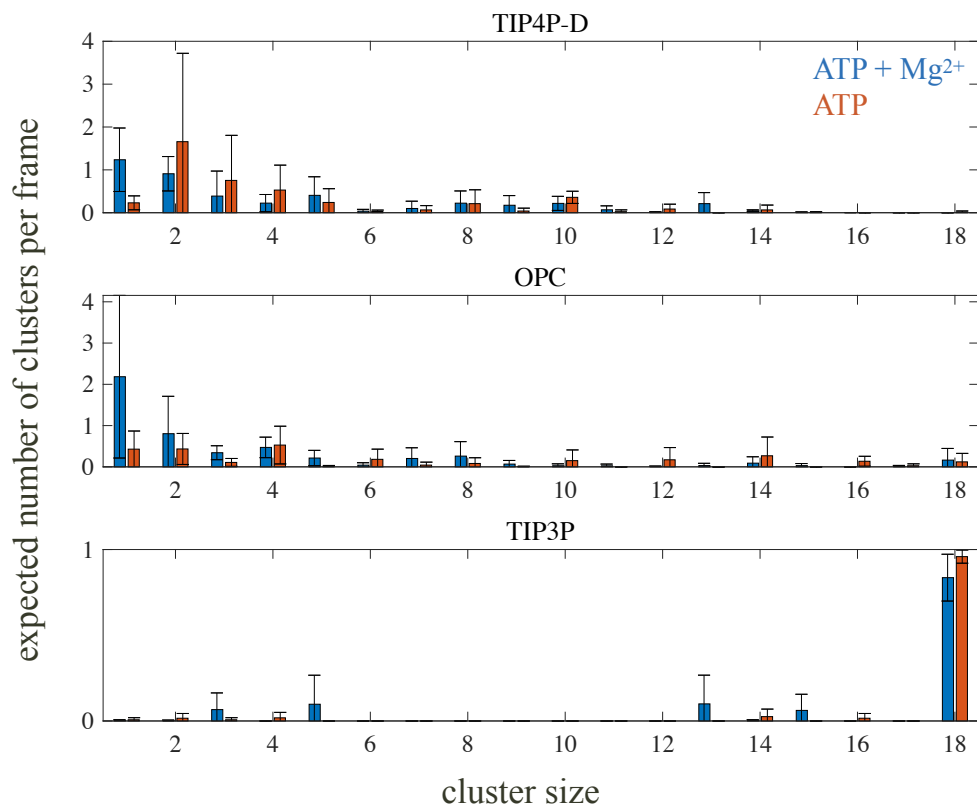
FIG. 2. Cluster size distributions averaged over the trajectories of ATP molecules in water. Top, center, and bottom figures are the results in TIP4P-D, OPC, and TIP3P waters, respectively. Blue and red bars denote the results with and without Mg^{2+} ions. The trajectory data from 0.2 to 1.2 μs of each trajectory are used for the time averages, and the three trajectories with different initial configurations are combined. The error bars are the standard deviations.

atomic distance between the two groups. The inter-triphosphate distance in the presence of Mg^{2+} shows a single peak at ~3 Å with a broad tail, implying that multiple conformations exist. This tail on the long-distance side becomes less obvious when Mg^{2+} is absent. The adenine-adenine distance, on the other hand, shows a sharp peak at ~3 Å, and additional peaks at 6, 9, and 12 Å. These secondary peaks are most obvious in the TIP3P water in the presnce of Mg^{2+}. This periodic character is indicative of the multiple π-π stacking layers, which can be confirmed in the snapshots (Fig. 4a). The snapshots of the clusters in the absence of Mg^{2+}, on the other hand, shows that a highly charged "core" consisting of many Na^+ ions and triphosphate groups are formed; this leads to the lack of long triphosphate-triphosphate distance and π-π stacking layers.

To see the stability of ATP–ATP contacts, we next analyze the lifetime of the ATP–ATP
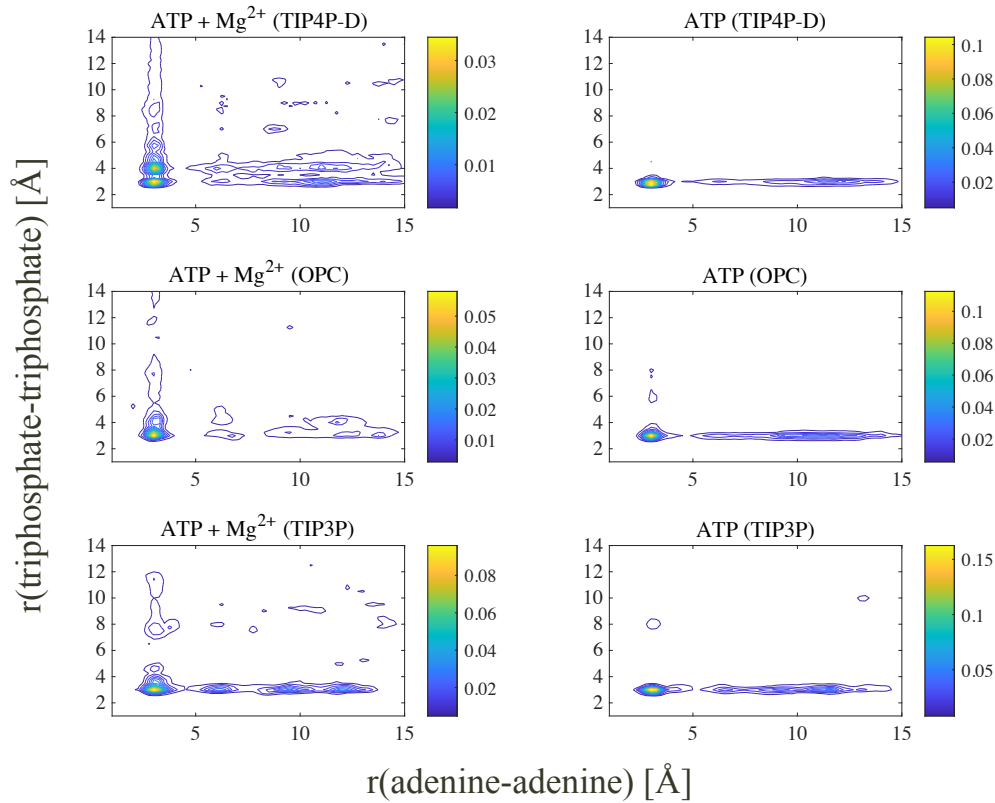
FIG. 3. Joint distributions of the adenine–adenine and triphosphate–triphosphate distances for all ATP pairs. Top, center, and bottom panels are the results for TIP4P-D, OPC, and TIP3P waters, respectively, and left and right columns describe the result with and without Mg^{2+} ions. Note that color ranges differ between the figures.

contact ($C_{\text{ATP}}(t)$), defined by the lifetime correlation function,

$$C_{\text{ATP}}(t) = \frac{1}{\displaystyle\sum_i^{\text{ATP}}\sum_{j>i}^{\text{ATP}} \langle \theta\left(r_0 - r_{ij}(\tau)\right)\rangle} \sum_i^{\text{ATP}}\sum_{j>i}^{\text{ATP}} \langle \theta\left(r_0 - r_{ij}(\tau)\right)\theta\left(r_0 - r_{ij}(\tau + t)\right)\rangle \qquad (1)$$

where t is the lag time, i and j denote the ATP molecules, and $\langle \cdots \rangle$ is the time average. $\theta(r_0 - r(t))$ is the binary function which becomes 1 when $r(t) \leq r_0$ and 0 otherwise, and r_0 is set to 4 Å. $C_{\text{ATP}}(t)$ thus describes the lifetime of a contact once it is formed. The result, given in Fig. 5, shows that the contacts are long-lived in the order of TIP3P > OPC > TIP4P-D. The large value of $C_{\text{ATP}}(t)$ for TIP3P even at 200 ns indicates that many contacts are kept preserved. This is consistent with the observation in Figs. 1, S2 and S3 that the cluster size in TIP3P water increase almost monotonically. We also see that the contacts are strengthened and become long-lived when Mg^{2+} ions are absent, which is also consistent
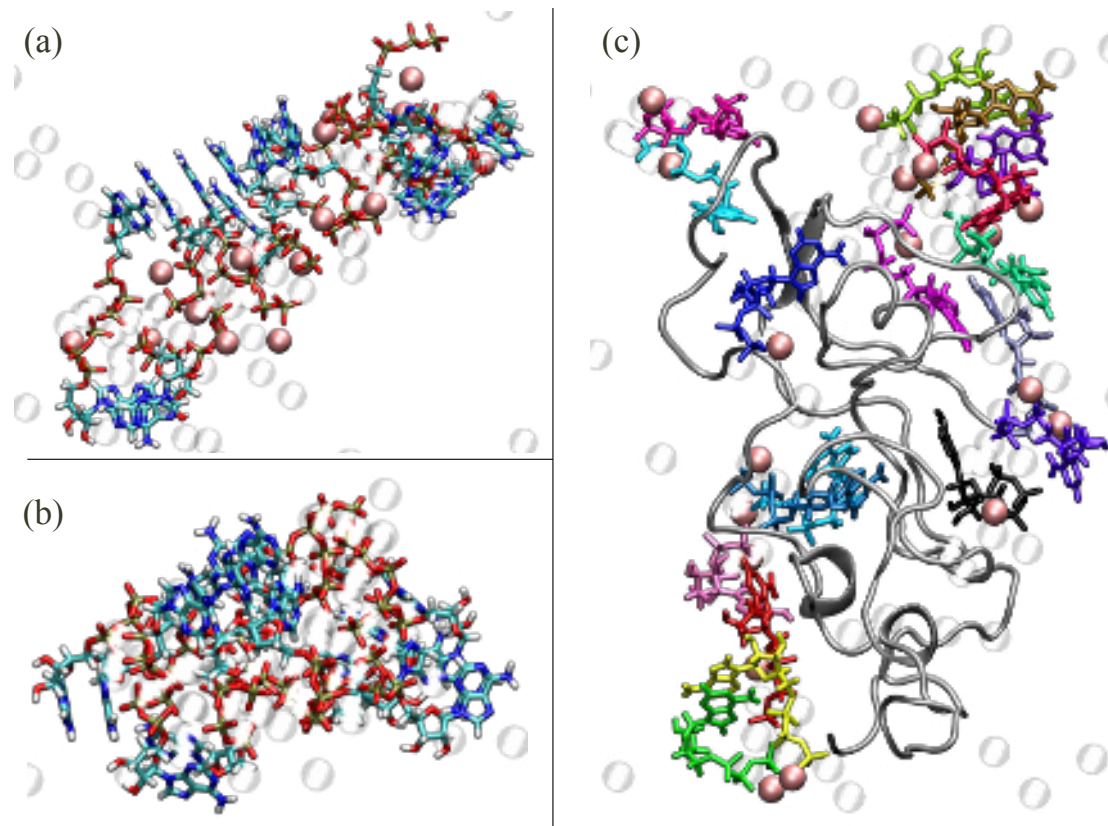
FIG. 4. Representative snapshots of (a) ATP and Mg^{2+}, (b) ATP without Mg^{2+}, and (c) α-Syn, ATP, and Mg^{2+} in TIP3P water. Pink and transparent balls are Mg^{2+} and Na^{+} ions, respectively. ATP and α-Syn are described in licorice and cartoon representations, respectively. Note that the patterns of the ATP–ATP interactions in different solvents are similar but the sizes of the clusters differ.

with the results discussed above.

ATP–α-Syn interactions

Next we analyze how ATP molecules interact with α-Syn. The time evolution of the shortest inter-atomic distances between the residues in α-Syn and the nearest ATP molecule for the representative trajectories are given in Fig. 6. The results for the other trajectories with and without Mg^{2+} ions are provided in Figs. S4 and S5, respectively. Fig. 6 shows that ATP molecules approach and leave α-Syn frequently in TIP4P-D water, whereas ATPs often stay nearby and contacts seem last for a few hundred nanoseconds in OPC water. The distances become even shorter in TIP3P water, i.e. almost all the residues are in close contact with ATP for most of the time. The absence of Mg^{2+} ions do not change these
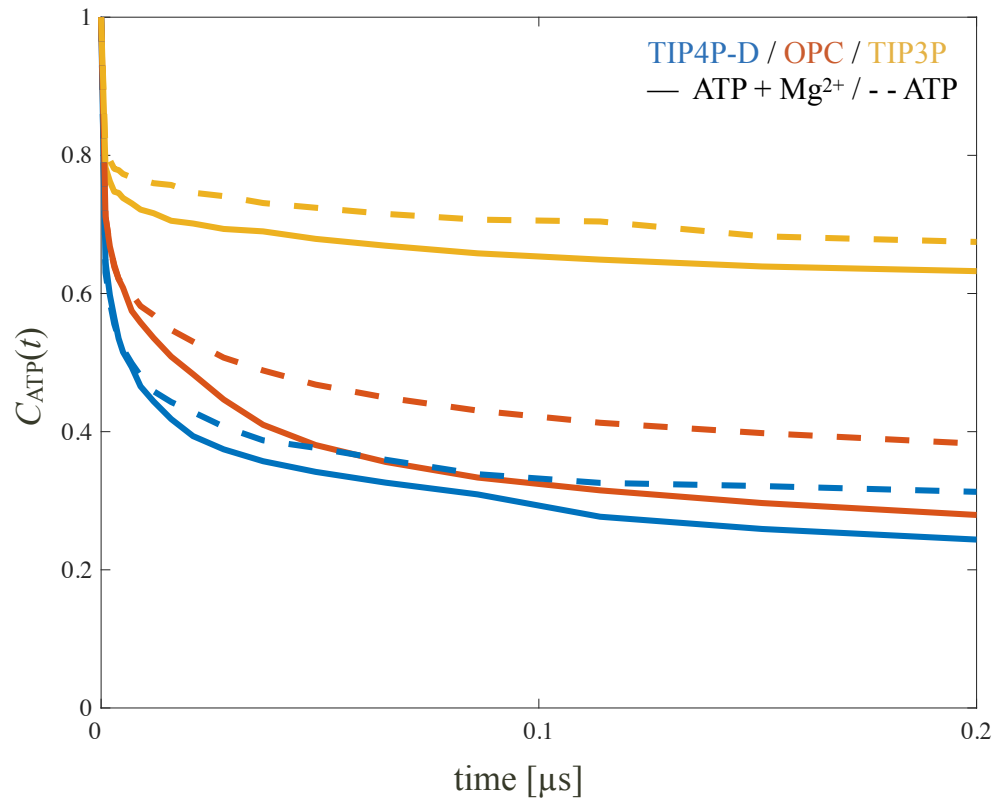
10

FIG. 5. Lifetime correlation functions of the ATP–ATP contacts with different waters. Blue, red, and yellow lines describe the results for TIP4P-D, OPC, and TIP3P waters, respectively, and solid and dashed lines denote the results with and without Mg^{2+} ions.

trends, though the chances of finding ATP molecules near α-Syn seems to increase slightly.

To understand the ATP–protein contacts in more detail, the probability of finding the ATP–protein contact for each residue is plotted in Fig. 7. The trajectory segments from 0.2 to 1.2 μs are used in time averaging to omit the drastic change of ATP distributions in the first 0.2 μs. The residue-ATP contact is counted when the shortest inter-atomic distance between the residue and an ATP is within 4 Å. The TIP4P-D result shows that stable contact is only occasionally found when Mg^{2+} is present (7.5 %, defined as an average over all residues), and the chances are only slightly increased when Mg^{2+} is absent (10.0 %). In the OPC water, on the other hand, ATP–protein contacts are formed more frequently, and the ratio increases when Mg^{2+} is absent (20.3 and 20.7 % for cases with and without Mg^{2+}, respectively). In contrast, strong contacts between ATP and α-Syn are seen in the TIP3P water even when Mg^{2+} ions are present (44.2 %), and the probability is almost unchanged when Mg^{2+} is replaced with Na^+ ions (43.0 %). The increase in the interactions in the
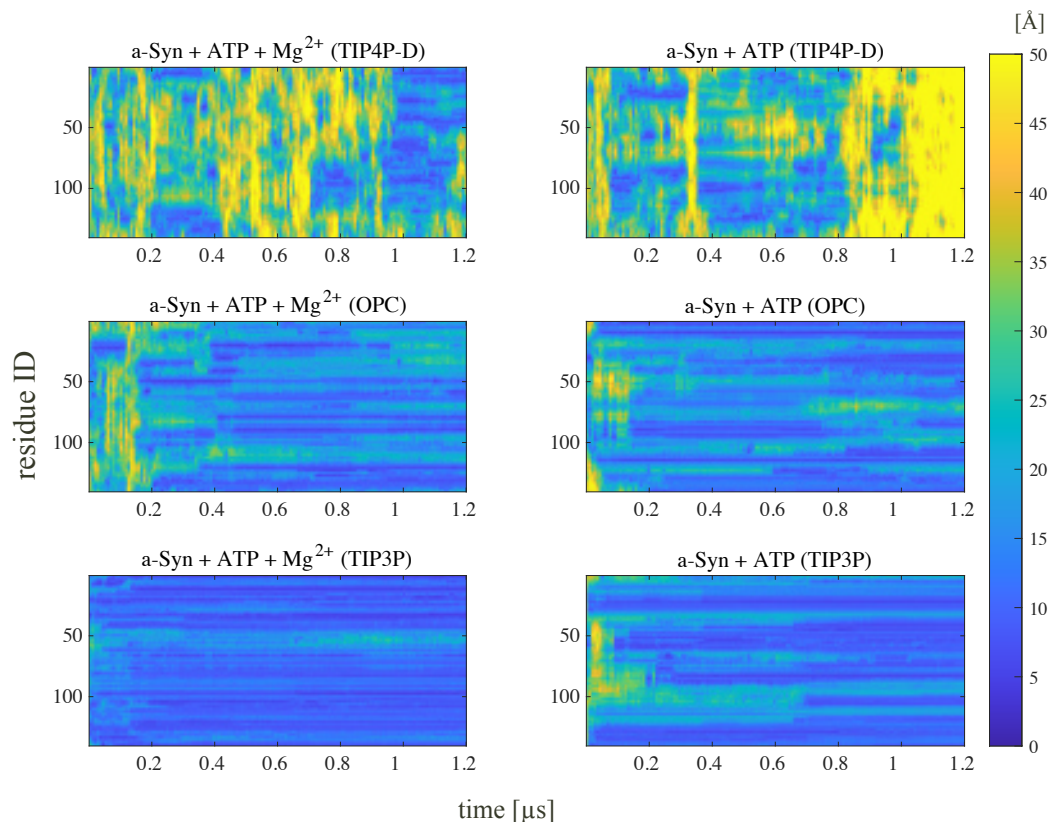
FIG. 6. Time evolution of the minimum distances between the residues in α-Syn and the ATP closest to each residue in the presence (left) and absence (right) of Mg^{2+}. Top, center, and bottom rows denote the results for TIP4P-D, OPC, and TIP3P waters, respectively.

absence of Mg^{2+} has also been observed in the NMR experiment[15]. However, we note that while the NMR experiment indicated that the effect of ATP is most notable at about the N-terminal (residues 113 to 137) and His50 (residues 49 to 52) moieties, the current results do not find clear preference to any regions. This may partly be due to the lack of sufficient conformational sampling of α-Syn, which is beyond the scope of the current work.

It has been suggested that Arg residues most frequently bind ATP molecules and mediate ATP–protein interactions in the protein native state.[17] Yet, α-Syn does not contain Arg. We thus examine which residue bind more frequently to ATPs. Fig. 8 shows the probability of residue–ATP contact formations for different residue names. The result shows that the residues containing a hydrophobic side chain in OPC water seem to bind ATP slightly more frequently than others. Charged residues in OPC water also seem to show slightly higher probability than the others. Yet, overall no clear preference to any residues is found.

To see the strength of residue-ATP contacts in further detail, the lifetime of the contacts
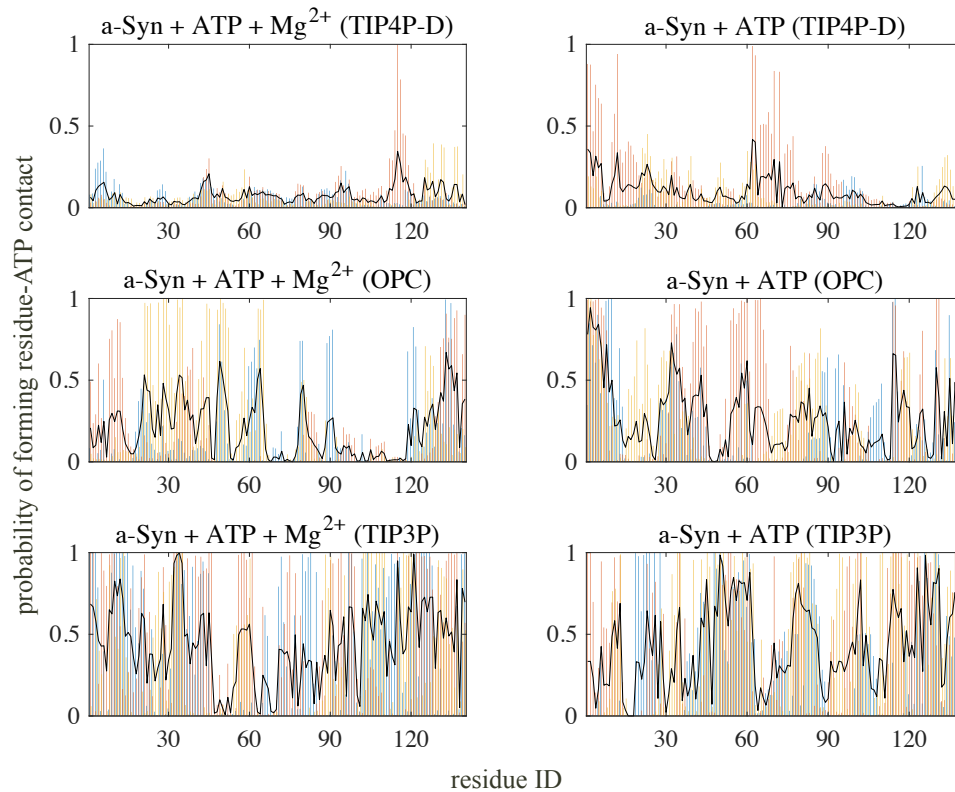
FIG. 7. The probability of finding the residue–ATP contacts during the trajectories. Top, center, and bottom rows are the results in TIP4P-D, OPC, and TIP3P water, respectively, and left and right columns are with and without Mg^{2+} ions. The bars in blue, red, and yellow are the results for the three trajectories from different initial structures, and the black lines shows the average over the three trajectories.

are analyzed with the lifetime correlation function ($C_{\text{type}}(t)$) similar to Eq. 1,

$$C_{\text{type}}(t) = \frac{1}{\sum\limits_{i \in \text{type}}^{\text{residue}} \sum\limits_{j}^{\text{ATP}} \langle \theta\left(r_0 - r_{ij}(\tau)\right) \rangle} \sum\limits_{i \in \text{type}}^{\text{residue}} \sum\limits_{j}^{\text{ATP}} \langle \theta\left(r_0 - r_{ij}(\tau)\right) \theta\left(r_0 - r_{ij}(\tau + t)\right) \rangle \quad (2)$$

where i and j denote the residues in α-Syn and ATP, respectively, and the cutoff distance (r_0) is set to 4 Å. To simplify the plot, the residues are classified into 5 types, i.e., positive (protonated His and Lys), negative (Asp and Glu), polar (Ser, Thr, Asn, and Gln), hydrophobic (Ala, Val, Ile, Leu, Met, Phe, and Tyr), and others (Gly and Pro). $C_{\text{type}}(t)$ is calculated as an average over the residues that belong to the same type. The result, given in Fig. 9, shows that all contacts behave similarly in TIP4P-D water, and decay within 0.1 μs when Mg^{2+} is present. Here, the absence of Mg^{2+} only slightly increases the lifetimes.
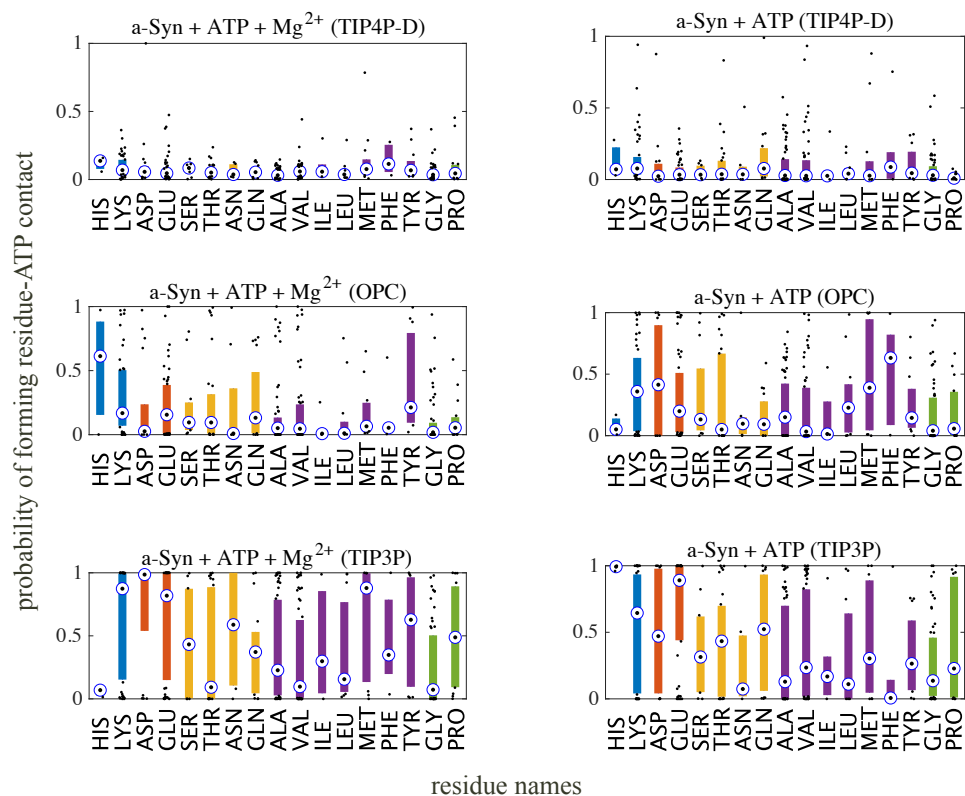
FIG. 8. Box plots for the probability of residue–ATP contacts formed throughout the trajectories, classified by residues names. Bottom and top edges of each box indicate the 25% and 75% ranges, respectively, and the outliers are shown in black points. Top, center, and bottom rows are for TIP4P-D, OPC, and TIP3P water results, respectively. Left and right columns are the results with and without Mg^{2+} ions. Dot plots shows the raw data for each residue, and stars denote the average over the residues. The colors of the dots denote the types of each residue. The positive, negative, polar, hydrophobic, and residual (other) residues are plotted in blue, red, yellow, purple, and green, respectively. Note that His residue is protonated, and Arg, Trp, and Cys residues are not included in α-Syn.

The contacts in OPC water show longer lifetimes compared to those in TIP4P-D, and do not decay to ~ 0 at 0.2 μs. The contacts between ATP and positively charged and polar residues tend to show slightly longer lifetimes. When Mg^{2+} is absent, $C_{\text{type}}(t)$ for both positively and negatively charged residues increase notably in the OPC result. This indicates that the contacts involving charged residues are stabilized. Finally, in TIP3P water, $C_{\text{type}}(t)$ changes quickly within 0.01 μs, but above 0.5 even at 0.2 μs. Together with Fig. 8, this result indicates that majority of the ATP–protein contacts are maintained in TIP3P water once they are formed. This trend is more apparent for the charged residues, and is further pronounced when Mg^{2+} is not involved in the system.
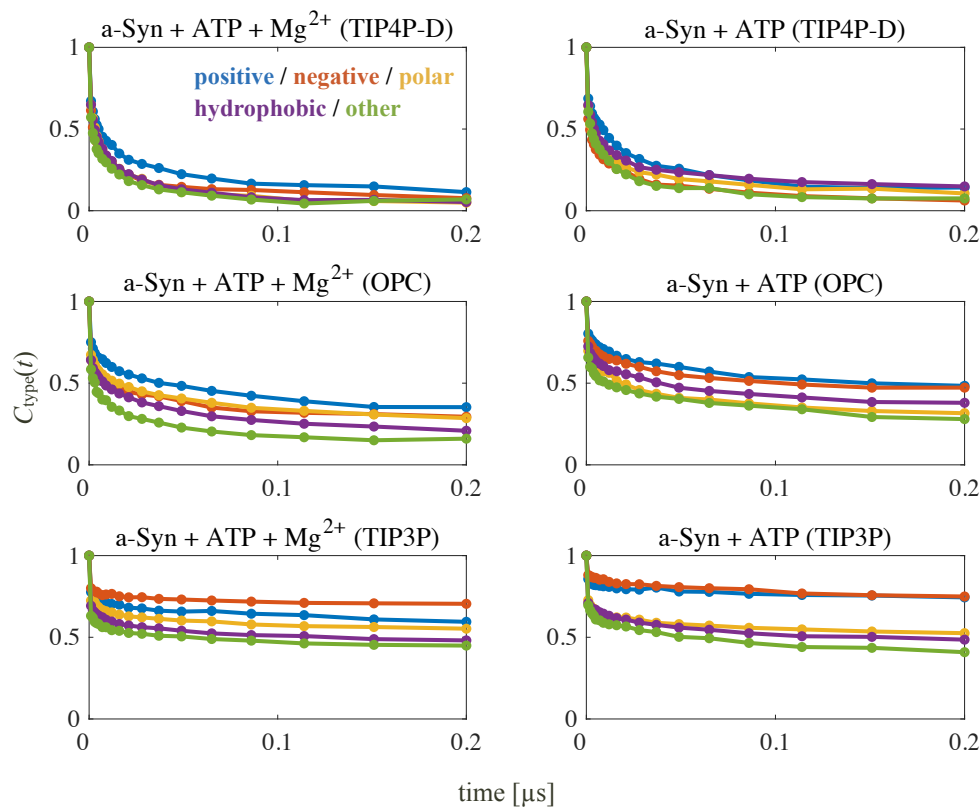
14

FIG. 9. Lifetime correlation functions of the ATP–protein contacts for residue types. Top, center, and bottom rows denote the results in TIP4P-D, OPC, and TIP3P waters, respectively, and left and right columns are for those with and without Mg^{2+}. The positive, negative, polar, hydrophobic, and residual (other) residues are plotted in blue, red, yellow, purple, and green, respectively.

To understand the molecular origin of the ATP–protein contacts, the joint probability distribution of the residue-triphosphate and residue-adenine distances between α-Syn and ATP molecules are plotted in Fig. 10. The distances denote the shortest inter-atomic distances between the two groups. This figure shows that the adenine moiety of ATP is frequently found within 4 Å of α-Syn. Notably, while we do see a peak where the triphosphate group is within 4 Å in the cases of OPC and TIP3P waters, this peak disappears in the 4P result. The TIP3P result further shows a peak where the contact is formed only via the triphosphate group, i.e., the residue-adenine and residue-triphosphate distances are peaked at $\sim$8 Å and $\sim$3 Å, respectively. When Mg^{2+} is absent, the protein-triphosphate interactions become stronger in all cases. In the OPC and TIP3P results, the triphosphate-mediated contacts, i.e., protein–triphosphate and protein–adenine distances are $\leq$ 4 Å and > 4 Å, respectively, show multiple peaks. This contact pattern is rarely seen in the TIP4P-D
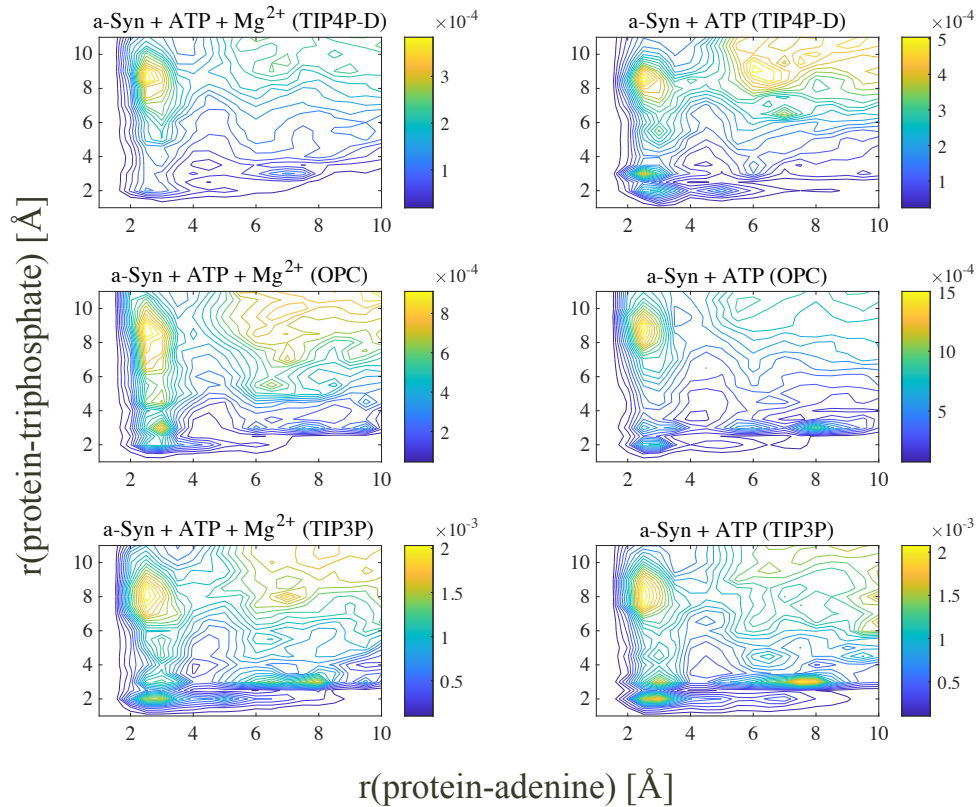
15

FIG. 10. The joint distributions of residue–triphosphate and residue–adenine distances. Top, center, and bottom rows are the results in the TIP4P-D, OPC, and TIP3P water, respectively, and left and right columns show those with and without Mg^{2+} ions. Note that color range differ between the figures.

result, indicating that the electrostatic interaction remains to be minor in TIP4P-D water.

Finally, we analyze the ATP clusters in the presence of α-Syn. Figs. S6 and S7 show the time evolution of the cluster sizes with and without Mg^{2+}, respectively. Fig. 11 summarizes the cluster size distributions, and Fig. 12 gives the lifetime correlation function ($C_{ATP}(t)$, Eq. 1) for the ATP–ATP contacts. Fig. 11 shows that the size distributions of the ATP clusters are broader than in the case without α-Syn (Fig. 2). This is even more pronounced in TIP3P water, i.e., multiple clusters are found. Yet, it turns out that these ATP clusters are bound to α-Syn, thus a large single cluster involving α-Syn is formed (Fig. 4c). In contrast, the ATPs in TIP4P-D water separate from α-Syn and exist as independent oligomers. The OPC result shows a trend in-between TIP4P-D and TIP3P. Finally, Figs. 11 and 12 indicate that ATP–ATP contacts tend to become stronger when Mg^{2+} is absent and the $C_{ATP}(t)$ behave similarly to those in the absence of α-Syn (Fig. 5). Thus, the character of the ATP–ATP
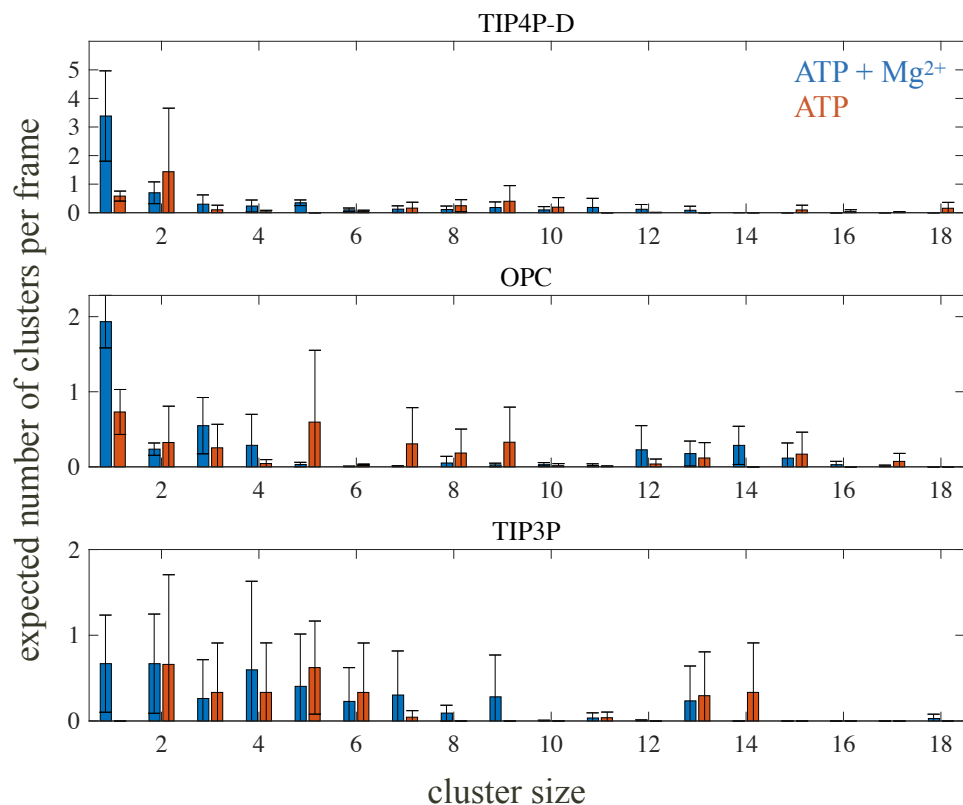
FIG. 11. Distributions of the expected sizes of ATP clusters in the presence of α-Syn. Top, center, and bottom panels are the results for TIP4P-D, OPC, and TIP3P waters, respectively. Blue and red plots denote the cases with and without Mg^{2+} ions. The error bars are the standard deviation estimated from the three trajectories.

interactions is largely unaffected by α-Syn.

IV. SUMMARY

In this study, we performed MD simulations of ATP molecules under different solvent environments to understand how the choice of water model affects ATP oligomerization and ATP binding to a disordered protein, α-Syn. Three water models, i.e., TIP4P-D, OPC, and TIP3P, were compared, and the effect of Mg^{2+} was also examined.

The common TIP3P water model was confirmed to highly overestimate the aggregation of ATPs regardless of Mg^{2+} ions. In contrast, the aggregation behavior was greatly reduced in TIP4P-D and OPC waters, and the monomeric state was found for 7 and 12 % of ATPs, respectively, in the presence of Mg^{2+} ions. When Mg^{2+} ions were replaced with Na^+ ions,
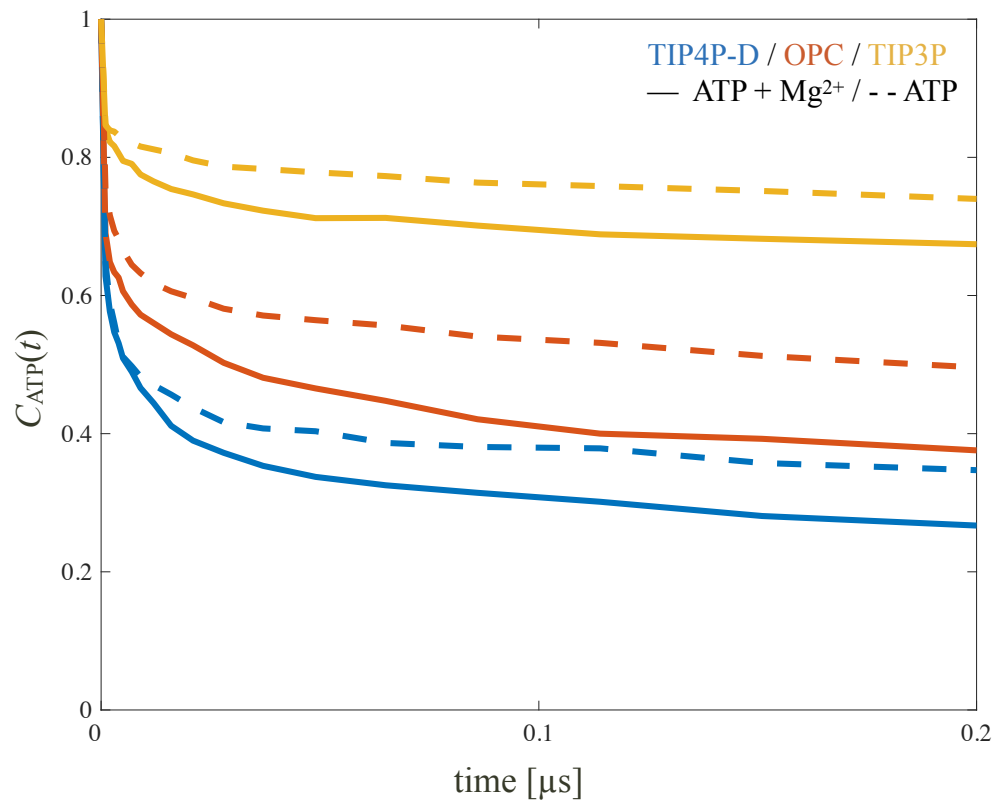
FIG. 12. Lifetime correlation functions of the ATP–ATP contacts in the presence of α-Syn. Blue, red, and yellow colors show the TIP4P-D, OPC, and TIP3P results, respectively, and solid and dashed lines are the results with and without Mg^{2+} ions.

oligomerization of ATP molecules were promoted. The ATP–ATP contacts were formed via both π-π (adenine–adenine) and electrostatic (triphosphate–triphosphate) interactions, where the latter was mediated by positively charged ions. Interestingly, the electrostatic interaction was found to become stronger when Mg^{2+} was absent, despite the fact that the positive charge on Na^+ is smaller than that on Mg^{2+}. Inspections of the trajectory snapshots indicated that while one divalent Mg^{2+} ion can stabilize the negatively-charged triphosphate group in ATP more effectively than a monovalent Na^+, multiple Na^+ ions gather around each triphosphate moiety and form a globular cluster containing multiple Na^+ ions and triphosphate groups when Mg^{2+} ions are absent. The globular structure resulted in shorter inter-triphosphate distances and larger ATP clusters.

The ATP distribution about α-Syn was also found to strongly depend on the water models. In particular, the binding of ATP molecules to α-Syn in TIP3P water was estimated to be very strong, i.e., more than half of the ATP–protein contacts were maintained for more

than 0.2 μs. In contrast, the ATP–protein contacts were formed only weakly in TIP4P-D water. In OPC water, more ATPs were bound to α-Syn compared to the case in TIP4P-D water, and the contact formation was promoted when Mg^{2+} was absent.

While previous study suggested that Arg residue is important for ATP–protein interactions in the protein native state, the intrinsically disordered protein α-Syn, which lack Arg, did not show clear preference for any residues. This may be because, unlike the native state where charged residues are often exposed to the surface, disordered protein is quite flexible such that ATP molecules can approach any residue with similar chance, thus hydrophobic residues can interact with ATPs more frequently. The ATP–hydrophobic residue interactions have also been found in previous studies on protein aggregates[21,23,24], and whether this feature is common in disordered proteins is left to be explored.

By analyzing the molecular origin of the ATP–protein contacts, the protein–adenine was found to be the dominant interaction. The contact mediated only via electrostatic interaction was also observed in TIP3P water in the presence of Mg^{2+}. When Mg^{2+} ions were absent, the protein-triphosphate contacts also became stable in OPC water, and the charged residues were found to form contacts with ATP more frequently and stably. These results indicate that the absence of Mg^{2+} increases the ATP–protein interactions, which is consistent with the previous NMR experiment.[15]

Here we note that the current work is intended to explore the effect of water models rather than quantifying the ATP–protein interactions. Nevertheless, the current results already show clear differences in the strength of ATP–protein interactions between the three water models. The TIP3P and TIP4P-D waters indicates that the interactions are nearly permanent and very weak, respectively, whereas the OPC model show modest interaction and repeated binding/unbinding events. The NMR experiment[15] have stated that the interactions are "weak and nonspecific", thus implies that TIP3P overestimates the ATP–protein interaction. Yet, to compare the water models quantitatively, the conformational space of the protein itself have to be explored in more detail. It has been shown that conformational sampling of α-Syn requires more than 10 μs-long trajectories[30], and discussing the slow ATP binding/unbinding events will need the trajectory to be even longer. It is thus expected that extensive conformational sampling of disordered proteins employing extended sampling methods are required to discuss the ATP–protein interactions in more detail.

Finally, previous studies have noticed that ATP molecules tend to over-aggregate in

TIP3P water, and have tuned the force field of ATP by scaling the charges to control oligomerization[19,20]. While such approach will also diminish the ATP–protein potential, here we showed that by merely changing the water model, the ATP over-aggregation trend can be reduced while keeping the ATP–protein potential unchanged. On the other hand, ATP in high concentration plays various roles by interacting with both native and disordered proteins. We also note that these water models have been recognized to destabilize the protein native states[30], and protein force fields to describe both the native and disordered states in a balanced manner have been thus been developed[42,43]. Since the ATP–protein interactions in high ATP concentrations have not been explored for these state-of-art force fields, a comprehensive study to reveal the ATP–protein interactions is necessary to reveal the role of ATP as a hydrotrope.

ACKNOWLEDGMENTS

SUPPLEMENTARY MATERIAL

Cartoon representations of the initial conformations of α-Synuclein, time evolution of the cluster sizes for ATP without protein and Mg^{2+} ions, time evolution of the minimum distances between the residues in α-Syn and ATP in the absence of Mg^{2+}, and time evolution of the cluster sizes found in the trajectories in the presence of α-Syn with and without Mg^{2+} ions.

DATA AVAILABILITY

The data that support the findings of this study are available from the corresponding author upon reasonable request.

REFERENCES

[1]W. Merlevede, J. R. Vandenheede, J. Goris, and S. Yang, "Regulation of atp–mg-dependent protein phosphatase," Current Topics in Cellular Regulation **23**, 177–215 (1984).

[2]T. W. Traut, "Physiological concentrations of purines and pyrimidines," Molecular and Cellular Biochemistry **140**, 1–22 (1994).

[3]N. Sakaki, R. Shimo-Kon, K. Adachi, H. Ito, S. Furuike, E. Muneyuki, M. Yoshida, and K. Kinosita, "One rotary mechanism for f1-atpase over atp concentrations from millimolar down to nanomolar," Biophysical Journal **88**, 2047–2056 (2005).

[4]J. V. Greiner and T. Glonek, "Hydrotropic function of atp in the crystalline lens," Experimental Eye Research **190**, 107862 (2020).

[5]A. Patel, L. Malinovska, S. Saha, J. Wang, S. Alberti, Y. Krishnan, and A. A. Hyman, "Atp as a biological hydrotrope," Science **356**, 753–756 (2017).

[6]S. Sridharan, N. Kurzawa, T. Werner, I. Gnthner, D. Helm, W. Huber, M. Bantscheff, and M. M. Savitski, "Proteome-wide solubility and thermal stability profiling reveals distinct regulatory roles for atp," Nature Communications **10**, 1155 (2019).

[7]J. Kang, L. Lim, and J. Song, "Atp binds and inhibits the neurodegeneration-associated fibrillization of the fus rrm domain," Communications Biology **2**, 223 (2019).

[8]F. Paoletti, F. Merzel, A. Cassetta, I. Ogris, S. Covaceuszach, J. Grdadolnik, D. Lamba, and S. G. Grdadolnik, "Endogenous modulators of neurotrophin signaling: Landscape of the transient atp-ngf interactions," Computational and Structural Biotechnology Journal **19**, 2938–2949 (2021).

[9]Z. Tian and F. Qian, "Adenosine triphosphate-induced rapid liquid-liquid phase separation of a model igg1 mab," Molecular Pharmaceutics **18**, 267–274 (2021).

[10]J. Kang, L. Lim, and J. Song, "Atp enhances at low concentrations but dissolves at high concentrations liquid-liquid phase separation (llps) of als/ftd-causing fus," Biochemical

and Biophysical Research Communications **504**, 545–551 (2018).

[11]J. Kang, L. Lim, Y. Lu, and J. Song, "A unified mechanism for llps of als/ftld-causing fus as well as its modulation by atp and oligonucleic acids," PLoS Biology **17**, e3000327 (2019).

[12]L. Wang, L. Lim, M. Dang, and J. Song, "A novel mechanism for atp to enhance the functional oligomerization of tdp-43 by specific binding," Biochemical and Biophysical Research Communications **514**, 809–814 (2019).

[13]C. Neuberg, "Hydrotropic phenomena. i," Biochem. Z. **76**, 107–176 (1916).

[14]J. Mehringer and W. Kunz, "Carl neuberg's hydrotropic appearances (1916)," Advances in Colloid and Interface Science **294**, 102476 (2021).

[15]M. Nishizawa, E. Walinda, D. Morimoto, B. Kohn, U. Scheler, M. Shirakawa, and K. Sugase, "Effects of weak nonspecific interactions with atp on proteins," Journal of the American Chemical Society **143**, 11982–11993 (2021).

[16]X. Ou, Y. Lao, J. Xu, Y. Wutthinitikornkit, R. Shi, X. Chen, and J. Li, "Atp can efficiently stabilize protein through a unique mechanism," JACS Au **1**, 1766–1777 (2021).

[17]G. Hu, X. Ou, and J. Li, "Mechanistic insight on general protein-binding ability of atp and the impacts of arginine residues," Journal of Physical Chemistry B **126**, 4647–4658 (2022).

[18]S. Sarkar and J. Mondal, "Mechanistic insights on atp's role as a hydrotrope," Journal of Physical Chemistry B **125**, 7717–7731 (2021).

[19]M. P. Pandey, S. Sasidharan, V. A. Raghunathan, and H. Khandelia, "Molecular mechanism of hydrotropic properties of gtp and atp," Journal of Physical Chemistry B **126**, 8486–8494 (2022).

[20]J. Mehringer, T. M. Do, D. Touraud, M. Hohenschutz, A. Khoshsima, D. Horinek, and W. Kunz, "Hofmeister versus neuberg: is atp really a biological hydrotrope?" Cell Reports Physical Science **2**, 100343 (2021).

[21]R. Roy and S. Paul, "Potential of atp toward prevention of hiapp oligomerization and destabilization of hiapp protofibrils: An in silico perspective," Journal of Physical Chemistry B **125**, 3510–3526 (2021).

[22]S. Pal and S. Paul, "Atp controls the aggregation of a16-22 peptides," Journal of Physical Chemistry B **124**, 210–223 (2020).

[23]I. Kurisaki and S. Tanaka, "Atp converts a42 oligomer into off-pathway species by making contact with its backbone atoms using hydrophobic adenosine," Journal of Physical Chemistry B **123**, 9922–9933 (2019).

[24]H. Aida, Y. Shigeta, and R. Harada, "The role of atp in solubilizing rna-binding protein fused in sarcoma," Proteins: Structure, Function and Bioinformatics **90**, 1606–1612 (2022).

[25]T. R. Sosnick and D. Barrick, "The folding of single domain proteinshave we reached a consensus?" Current Opinion in Structural Biology **21**, 12–24 (2011).

[26]S. Piana, J. L. Klepeis, and D. E. Shaw, "Assessing the accuracy of physical models used in protein-folding simulations: Quantitative evidence from long molecular dynamics simulations," Current Opinion in Structural Biology **24**, 98–105 (2014).

[27]P. S. Nerenberg, B. Jo, C. So, A. Tripathy, and T. Head-Gordon, "Optimizing SoluteWater van der Waals Interactions To Reproduce Solvation Free Energies," J. Phys. Chem. B **116**, 4524–4534 (2012).

[28]R. B. Best, W. Zheng, and J. Mittal, "Balanced ProteinWater Interactions Improve Properties of Disordered Proteins and Non-Specific Protein Association," J. Chem. Theory Comput. **10**, 5113–5124 (2014).

[29]D. Song, R. Luo, and H.-F. Chen, "The IDP-Specific Force Field ff14IDPSFF Improves the Conformer Sampling of Intrinsically Disordered Proteins," J. Chem. Inf. Model. **57**, 1166–1178 (2017).

[30]S. Piana, A. G. Donchev, P. Robustelli, and D. E. Shaw, "Water dispersion interactions strongly influence simulated structural properties of disordered protein states," Journal of Physical Chemistry B **119**, 5113–5123 (2015).

[31]P. S. Shabane, S. Izadi, and A. V. Onufriev, "General purpose water model can improve atomistic simulations of intrinsically disordered proteins," Journal of Chemical Theory and Computation **15**, 2620–2634 (2019).

[32]L. Martinez, R. Andrade, E. G. Birgin, and J. M. Martnez, "Packmol: A package for building initial configurations for molecular dynamics simulations," Journal of Computational Chemistry **30**, 2157–2164 (2009).

[33]K. Lindorff-Larsen, S. Piana, K. Palmo, P. Maragakis, J. L. Klepeis, R. O. Dror, and D. E. Shaw, "Improved side-chain torsion potentials for the amber ff99sb protein force field," Proteins: Structure, Function and Bioinformatics **78**, 1950–1958 (2010), amber FF99SB-ILDN parameter.

[34]K. L. Meagher, L. T. Redman, and H. A. Carlson, "Development of polyphosphate parameters for use with the amber force field," Journal of Computational Chemistry **24**, 1016–1025 (2003), aMBER phosphate parameters.

[35]I. S. Joung and T. E. Cheatham, "Determination of alkali and halide monovalent ion parameters for use in explicitly solvated biomolecular simulations," Journal of Physical Chemistry B **112**, 9020–9041 (2008).

[36]Z. Li, L. F. Song, P. Li, and K. M. Merz, "Systematic parametrization of divalent metal ions for the opc3, opc, tip3p-fb, and tip4p-fb water models," Journal of Chemical Theory and Computation **16**, 4429–4442 (2020).

[37]D. A. Case, K. Belfon, I. Y. Ben-Shalom, S. R. Brozell, D. S. Cerutti, V. W. D. Cruzeiro, T. A. Darden, R. E. Duke, and G. Giambasu, "Amber 20,".

[38]R. Salomn-Ferrer, A. W. Goetz, D. Poole, S. L. Grand, and R. C. Walker, "Routine microsecond molecular dynamics simulations with amber on gpus. 2. explicit solvent particle mesh ewald," Journal of Chemical Theory and Computation **9**, 3878–3888, reference for the GPU version of Amber 12.

[39]K. H. Scheller, F. Hofstetter, P. R. Mitchell, B. Prijs, and H. Sigel, "Macrochelate formation in monomeric metal ion complexes of nucleoside 5'-triphosphates and the promotion of stacking by metal ions. comparison of the self-association of purine and pyrimidine 5'-triphosphates using proton nuclear magnetic resonance," Journal of the American Chemical Society **103**, 247–260 (1981).

[40]J. E. Wilson and A. Chin, "Chelation of divalent cations by atp, studied by titration calorimetry," Analytical Biochemistry **193**, 16–19 (1991).

[41]A. C. Storer and A. Cornish-Bowden, "Concentration of mgatp2- and other ions in solution. calculation of the true concentrations of species present in mixtures of associating ions," Biochemical Journal **159**, 1–5 (1976).

[42]J. Huang, S. Rauscher, G. Nawrocki, T. Ran, M. Feig, B. L. de Groot, H. Grubmller, and A. D. MacKerell, "Charmm36m: an improved force field for folded and intrinsically disordered proteins," Nature Methods **14**, 71–73 (2017).

[43]P. Robustelli, S. Piana, and D. E. Shaw, "Developing a molecular dynamics force field for both folded and disordered protein states," Proc. Natl. Acad. Sci. U. S. A. **115**, E4758–E4766 (2018).